



Electrocatalytic property, anticancer activity, and density functional theory calculation of $[\text{NiCl}(\text{P}^{\wedge}\text{N}^{\wedge}\text{P})]\text{Cl}\cdot\text{EtOH}$

Gholamhossein Mohammadnezhad¹  | Saeed Abad¹ | Hossein Farrokhpour¹ | Helmar Görls² | Winfried Plass² 

¹Department of Chemistry, Isfahan University of Technology, Isfahan, 84156-83111, Islamic Republic of Iran

²Institute of Inorganic and Analytical Chemistry, Friedrich-Schiller-Universität Jena, Humboldtstr. 8, Jena, 07743, Germany

Correspondence

Gholamhossein Mohammadnezhad, Department of Chemistry, Isfahan University of Technology, Isfahan 84156-83111, Islamic Republic of Iran. Email: mohammadnezhad@iut.ac.ir

Funding information

Research Affairs Division of Isfahan University of Technology (IUT); Iran National Science Foundation (INSF), Grant/Award Number: 94005007

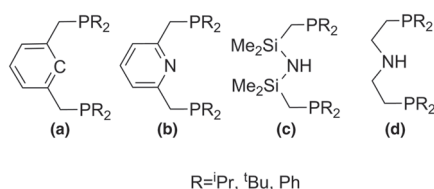
This study describes the electrocatalytic, anticancer, and density functional theory (DFT) studies of a nickel complex, $[\text{NiCl}(\text{P}^{\wedge}\text{N}^{\wedge}\text{P})]\text{Cl}\cdot\text{EtOH}$, based on a neutral $\text{P}^{\wedge}\text{N}^{\wedge}\text{P}$ -type pincer ligand ($\text{P}^{\wedge}\text{N}^{\wedge}\text{P}$ = bis[(2-diphenylphosphino)ethyl] amine). The ligand was synthesized without time-consuming and costly amine protection. It was characterized by ^1H NMR, ^{31}P NMR, Fourier transform infrared (FT-IR), UV-vis, and single-crystal X-ray diffraction. The complex was isolated as a solvated chloride salt and characterized by FT-IR, UV-visible, ^1H NMR, ^{13}C NMR, and ^{31}P NMR spectroscopies as well as single-crystal X-ray diffraction and CHN analysis. The ligand and complex crystallized in a monoclinic $P2_1/c$ space group. The molecular structure of the complex contains a four-coordinated distorted nickel ion with square-planar geometry. The electrocatalytic hydrogen ion reduction was studied for the nickel complex in an acidic non-aqueous medium. Cyclic voltammetry studies showed that this complex is an efficient electrocatalyst for hydrogen evolution at the potential of the $\text{Ni}(\text{II/I})$ couple. As a potential anticancer agent, the biological activities of the Ni complex were tested against two human cancer cell lines (MCF7 and HT29). The IC_{50} results demonstrated that the nickel complex has better cytotoxic activity than *cis*-platin against the human breast cancer cell (MCF7) line. DFT calculations were performed to study the kinetics and thermodynamics of the pincer ligand's synthetic procedure and its Ni complex. Time-dependent DFT calculations were performed to calculate the pincer ligand's UV-vis spectra and the complex, which was in agreement with the experimental data. To assign the calculated UV spectra, molecular orbital calculations were performed. Finally, a modified mechanism was proposed for the electrocatalytic hydrogen ion reduction by $[\text{Ni}(\text{P}^{\wedge}\text{N}^{\wedge}\text{P})\text{Cl}]\text{Cl}\cdot\text{EtOH}$. The theoretical calculations showed that the cycle is thermodynamically favorable.

KEYWORDS

aliphatic $\text{P}^{\wedge}\text{N}^{\wedge}\text{P}$ ligand, anticancer, electrocatalyst, pincer complex, theoretical calculation

1 | INTRODUCTION

Pincer-type molecules/ions are an exciting class of ligands that have received increasing attention in modern organometallic chemistry.^[1–3] Metal complexes of pincer-type ligands have been successfully employed for a wide variety of applications including supramolecular chemistry,^[4–6] antibacteria,^[7] anticancer,^[8–12] sensors,^[13,14] and of course for catalytic reactions (heterogenic and homogenic).^[15–24] The earliest synthesis of these ligands dates back to 1976 but it wasn't until in 1989 that van Koten applied the term “pincer” word for this group of ligands.^[25,26] Since then, these ligands have found wide usage for specific purposes in the chemical sciences.^[26] The formation of such complexes possessing high thermal stability and reactivity is a consequence of pincer ligand contribution.^[27] Tridentate pincer ligands having the description P^YY^P (where Y = heteroatom), are tridentate and have been reported with *meridional* geometry at the metal center.^[28,29] In addition, the successful synthesis of pincer ligands is dependent on factors such as nature of heteroatom (Y), type of solvent, and electron-donating or electron-withdrawing group on the Y atom.^[30] Some typical P^YY^P pincer ligands are shown in Scheme 1. Among these, ligands with aromatic centers, P^CC^P and P^NN^P (Scheme 1a,b), represent the most widely used structures where the aryl backbone leads to stability and rigidity.^[31–34] Reports indicated that the synthetic mechanism of these ligands was followed by S_N2 nucleophilic substitution.^[30,35,36] Fryzuk first reported the synthesis of a less common PNP pincer ligand possessing a central amino group (Scheme 1c) in the 1980s.^[37] Aliphatic P^NN^P pincer ligands (Scheme 1d) were first reported by Danopoulos and Edwards^[38] and later developed for their unique application as catalysts.^[39,40] There is a substantial difference between P^NN^P and P^CC^P ligands. For instance, nitrogen possesses a π -donor character resulting in the PNP ligands having a weaker *trans*-effect than the PCP types with the attendant result of increasing thermodynamic stability of the ligands.^[36] Nickel complexes of pincer ligands can also act as electrocatalysts for hydrogen ion reduction and are suitable for producing hydrogen as a green energy resource with low cost and high efficiency.^[41–43]



SCHEME 1 Some representative types of pincer ligands

Moreover, Lindley et al. synthesized rhenium complexes based on an aliphatic PNP ligand (N(CH₂CH₂P^{*t*}Bu₂)₂) and studied the electrochemical splitting of N₂ into the terminal nitride.^[44] Also, there are many reports about metal complexes with central metal ions such as Co(II), Ni(II), Cu(II), and Zn(II) that have been shown to display anticancer, antifungal, antibacterial, and antiviral activity.^[45–47] Among these, there has been growing interest in using nickel complexes in biological and pharmaceutical activities. Most of the investigated complexes with tridentate PNP ligands showed square-planar structures with high stability.^[48–53] In 2014, Milenković et al. synthesized square-planar Ni(II) complexes with P^NN^O tridentate ligands which show moderate antibacterial and cytotoxic activity.^[54]

In this paper, an aliphatic-centered pincer ligand (P^NN^P), as well as its nickel complex, was synthesized and characterized. The nickel complex of the pincer ligand acts as an efficient electrocatalyst for hydrogen ion reduction. Also, kinetics, thermodynamics, and orbital properties have been studied by theoretical calculation. Furthermore, the anticancer activities of [NiCl(P^NN^P)] Cl.EtOH were investigated using MCF7 (breast) and HT29 (colon) cancer cells.

2 | EXPERIMENTAL

2.1 | General procedures

Anhydrous solvents, including dichloromethane, *n*-hexane, tetrahydrofuran (thf), and ethanol, were prepared by the standard methods^[55] and degassed and stored in Schlenk tubes (the air was rigorously removed by three cycles of freeze–pump–thaw treatment). All experiments were carried out using standard Schlenk techniques under an argon atmosphere. Water was degassed by bubbling with argon before use. Chlorodiphenylphosphine and bis(2-chloroethyl)amine hydrochloride were purchased from Merck and used without further purification. Fourier transform infrared (FT-IR) spectra were recorded on a Jasco-680 spectrometer in the wavelength range between 400 cm^{–1} to 4000 cm^{–1}, using a KBr pellet and making 60 scans at 4 cm^{–1} resolution. The NMR spectra were recorded on a Varian MERCURY plus-400 (¹H: 300 MHz, ³¹P: 121 MHz) and Bruker ultra shield (¹H: 400 MHz, ³¹P: 162 MHz) spectrometer with chemical shifts reported in ppm relative to the residual deuterated solvents. Absorbance spectra were recorded on a UV–visible Jasco V-570 spectrophotometer using quartz cells of 1.0-cm optical path length in ethanol.

2.2 | Structure determinations

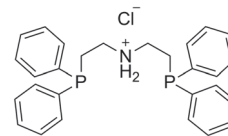
The intensity data for the compounds were collected on a Nonius KappaCCD diffractometer using graphite-monochromated Mo-K α radiation. Data were corrected for Lorentz and polarization effects; absorption was taken into account on a semi-empirical basis using multiple scans.^[56–58] The structures were solved by direct methods (SHELXS^[59]) and refined by full-matrix least-squares techniques against F_o^2 (SHELXL-2018^[60]). The hydrogen atoms bonded to the amine-groups N1 of both compounds were located by difference Fourier synthesis and refined isotropically. All other hydrogen atoms were included at calculated positions with fixed thermal parameters. All nonhydrogen atoms were refined anisotropically.^[60] MERCURY was used for structure representations.^[61]

Crystal data for $P^{\wedge}N^{\wedge}P.HCl$: $C_{28}H_{30}ClNP_2$, $M_r = 477.92 \text{ g mol}^{-1}$, colorless prism, size $0.122 \times 0.112 \times 0.108 \text{ mm}^3$, monoclinic, space group $P2_1/c$, $a = 10.1149(3)$, $b = 26.7526(7)$, $c = 10.2717(3) \text{ \AA}$, $\beta = 114.210(1)^\circ$, $V = 2535.06(13) \text{ \AA}^3$, $T = -140^\circ\text{C}$, $Z = 4$, $\rho_{\text{calcd.}} = 1.252 \text{ g cm}^{-3}$, $\mu (\text{Mo-K}\alpha) = 2.93 \text{ cm}^{-1}$, multiscan, $\text{trans}_{\text{min}}: 0.6579$, $\text{trans}_{\text{max}}: 0.7456$, $F(000) = 1008$, 17,501 reflections in $h(-13/13)$, $k(-34/34)$, $l(-13/13)$, measured in the range $2.208^\circ \leq \theta \leq 27.464^\circ$, completeness $\theta_{\text{max}} = 99.3\%$, 5747 independent reflections, $R_{\text{int}} = 0.0576$, 4749 reflections with $F_o > 4\sigma(F_o)$, 297 parameters, 0 restraints, $R^1_{\text{obs}} = 0.0607$, $wR^2_{\text{obs}} = 0.1401$, $R^1_{\text{all}} = 0.0760$, $wR^2_{\text{all}} = 0.1486$, GOOF = 1.078, largest difference peak and hole: $1.907/-0.499 \text{ e \AA}^{-3}$.

Crystal data for $[Ni(P^{\wedge}N^{\wedge}P)Cl].EtOH$: $C_{30}H_{35}Cl_2NNiOP_2$, $M_r = 617.14 \text{ g mol}^{-1}$, brown prism, size $0.132 \times 0.122 \times 0.105 \text{ mm}^3$, monoclinic, space group $P2_1/c$, $a = 15.4956(4)$, $b = 9.1535(3)$, $c = 23.7002(6) \text{ \AA}$, $\beta = 103.971(2)^\circ$, $V = 3262.17(16) \text{ \AA}^3$, $T = -140^\circ\text{C}$, $Z = 4$, $\rho_{\text{calcd.}} = 1.257 \text{ g cm}^{-3}$, $\mu (\text{Mo-K}\alpha) = 8.79 \text{ cm}^{-1}$, multiscan, $\text{trans}_{\text{min}}: 0.6314$, $\text{trans}_{\text{max}}: 0.7456$, $F(000) = 1288$, 38,930 reflections in $h(-20/20)$, $k(-11/11)$, $l(-30/30)$, measured in the range $1.952^\circ \leq \theta \leq 27.482^\circ$, completeness $\theta_{\text{max}} = 99.7\%$, 7439 independent reflections, $R_{\text{int}} = 0.0641$, 5604 reflections with $F_o > 4\sigma(F_o)$, 351 parameters, 18 restraints, $R^1_{\text{obs}} = 0.0922$, $wR^2_{\text{obs}} = 0.2390$, $R^1_{\text{all}} = 0.1230$, $wR^2_{\text{all}} = 0.2663$, GOOF = 1.104, largest difference peak and hole: $1.843/-0.726 \text{ e \AA}^{-3}$.

2.3 | Synthesis of bis[(2-diphenylphosphino)ethyl]ammonium chloride ($P^{\wedge}N^{\wedge}P.HCl$)

The ligand was synthesized by a modified reported procedure.^[62] The ligand has been shown in Scheme 2.



SCHEME 2 Bis[(2-diphenylphosphino)ethyl]ammonium chloride ($P^{\wedge}N^{\wedge}P.HCl$)

Chlorodiphenylphosphine (4 mmol, 640 μl) was added dropwise via a septum to a suspension of lithium granules (10 mmol, 0.073 g) in thf (5 ml) under argon atmosphere (Caution! The N_2 atmosphere reacts with lithium). The resulting solution was stirred vigorously at room temperature for 24 h to yield a deep red solution of lithium diphenylphosphanide. Then, this solution was transferred to the suspension of bis(2-chloroethyl)amine hydrochloride (1 mmol, 0.159 g) in thf (7 ml) by a cannula syringe. The reaction mixture was refluxed for 24 h. The resulting red solution was cooled down to room temperature. Subsequently, *n*-hexane (8 ml), 10% sodium hydroxide ($2 \times 2 \text{ ml}$), and saturated sodium chloride ($2 \times 2 \text{ ml}$) were added to the above solution, and the aqueous layer was removed. The organic layer was stirred for 45 min with HCl (2 M), and a white precipitate was collected by filtration over sintered glass. The white solid was purified in dichloromethane and diethyl ether. $C_{28}H_{30}ClNP_2$ ($477.92 \text{ g mol}^{-1}$). FT-IR (KBr, cm^{-1}): 3435 ($-\text{NH}_2$), 3100 (aromatic CH), 2923 ($-\text{CH}_2-$). UV-vis ($1.0 \times 10^{-4} \text{ mol L}^{-1}$; EtOH): $\lambda_{\text{max}} = 248 \text{ nm}$. ^1H NMR (400 MHz, CDCl_3 , 25°C , ppm): 2.65 and 2.85 (2 br s, 8H), 7.16–7.34 (m, 20H, Ph), 9.89 (s, 2H, NH_2). ^{31}P NMR (162 MHz, CDCl_3 , 25°C , ppm): -21 .

2.4 | Synthesis of $[Ni(P^{\wedge}N^{\wedge}P)Cl].Cl.EtOH$

The $P^{\wedge}N^{\wedge}P.HCl$ (0.047 g, 0.1 mmol) was dissolved in ethanol (2 ml) and added dropwise into a solution of nickel chloride (0.013, 0.1 mmol) in ethanol (2 ml) and stirred at room temperature for 2 h. An orange crystalline product was obtained by slow evaporation at 5°C . $C_{28}H_{29}Cl_2NNiP_2.C_2H_5OH$ ($617.14 \text{ g mol}^{-1}$). CHN: Calc: C, 58.38; H, 5.72; N, 2.27 Found: C, 57.85; H, 5.32; N, 2.56. FT-IR (KBr, cm^{-1}): 3410 (NH), 3100 (aromatic CH), 2923 ($-\text{CH}_2-$), 1481, 1434, 1172, 1101.15, 839, 748, 724, 693, 547, 498. UV-vis ($1.0 \times 10^{-4} \text{ mol L}^{-1}$; EtOH): $\lambda_{\text{max}} = 471 \text{ nm}$. ^1H NMR (300 MHz, CDCl_3 , 25°C , ppm): 2.16–2.52 (m, 4H, CH_2), 2.98–3.22 (m, 4H, CH_2), 7.4–8.3 (m, 20H, Ph), 10.44 (br s, NH). ^{13}C NMR (75 MHz, CDCl_3 , 25°C , ppm): 28.8 and 51.5 ($-\text{CH}_2-$), 129.3 (d, $J_{\text{C,P}} = 31 \text{ Hz}$), 131.7 (d, $J_{\text{C,P}} = 50 \text{ Hz}$), 133.5 (d, $J_{\text{C,P}} = 81 \text{ Hz}$) (aromatic). ^{31}P NMR (121 MHz, CDCl_3 , 25°C , ppm): 28.

2.5 | Electrochemical experiments

The electrocatalytic properties of $[\text{Ni}(\text{P}^{\wedge}\text{N}^{\wedge}\text{P})\text{Cl}]\text{Cl}\cdot\text{EtOH}$ (1 mM in acetonitrile) was studied in the presence of NBu_4BF_4 (0.1 M) as the supporting electrolyte. Cyclic voltammograms (CVs) were recorded using OGF500 Origaflex–Origalys at a scan rate of 30, 50, 100, and 150 mV s^{-1} . A typical three-electrode electrochemical system was used at room temperature and under argon atmosphere. It consists of a glassy carbon electrode, a platinum wire counter electrode, and a silver wire reference. Catalytic hydrogen evolution experiments were investigated after additions of 15, 65, 80, and 100 μl of 1 M HCl via syringe, and the CVs were recorded under an argon atmosphere. The agitation was provided by a small magnetic stirrer.

2.6 | Biological studies

The human colon adenocarcinoma cell line HT29 and human breast adenocarcinoma cell line MCF7 were cultured in Dulbecco's modified Eagle's medium (DMEM-low glucose, Bioidea-Iran) under a humidified atmosphere (95% air and 5% CO_2) at 37°C. The medium contained 10% fetal bovine serum (FBS) and 1% penestrep (penicillin and streptomycin).

2.7 | MTT cytotoxicity assay

The aliphatic pincer complex's cytotoxicity was investigated using adherent growing cell lines method with MTT (3-(4,5-dimethylthiazol-2-yl)-2,5-diphenyltetrazolium bromide) test. Three concentrations, 50, 100, and 200 μM , of each powder (*cis*-platin or Ni complex) was prepared in a culture medium-0.05% volume of ethanol (medium containing DMEM-low + 10% FBS + 1% penestrep) at 37°C in a humidified atmosphere with 5% CO_2 . MCF7 and HT29 cells were cultured with a growing density of 1.5×10^4 cells per well into a 97-well plate in order to expand the cells. After a day of culture, *cis*-platin and the pincer complex prepared in the culture medium were added to MCF7 and HT29 cells and then incubated at 37°C. MCF7 and HT29 cells were growing on tissue culture polystyrene (TCP) dishes without any additive in culture medium as control. After 24 and 48 h of incubation, the cell culture medium was removed, the pits were washed with phosphate-buffered saline, and cell durability rate was measured using the MTT test. In this regard, after incubation of the cells with MTT solution (0.5-mg ml^{-1} MTT reagent in PBS) for 4 h, DMSO was added to dissolve the purple MTT formazan crystals.

The 96-well plates were then read at 490 nm by using a Microplate Reader (Bio Rad, Model 680 instruments). For each sample, the final results were expressed using IC_{50} , a parameter that indicated the anticancer potency of chemicals.

2.8 | Computational methods

All calculations were carried out using the Gaussian 09 program,^[63] and the structures of ligand and nickel complex were optimized using the density functional theory (DFT) method employing B3PW91 functional. The standard 6-31G(d) basis set was adopted for H, C, N, P, and Cl atoms and LANL2DZ for the nickel atom. Also, the kinetics and thermodynamics of ligand synthesis were studied separately using the same computational method in the gas phase and thf, which was considered a polarized continuum solvent. The reaction rate was calculated by the equation presented in Mohammadnezhad et al.^[36]

The entropy of solvation (S_{solv}) can be calculated by Equation 1, which leads to the more accurate ΔG and ΔG^\ddagger of the reaction in the presence of thf.^[26,64]

$$\Delta S_{\text{solv}} = R \ln \frac{V_{\text{m,liquid}}}{V_{\text{m,gas}}} - \alpha \left(S^\circ + R \ln \frac{V_{\text{m,liquid}}}{V_{\text{m,gas}}} \right) + 7.98 \text{ cal mol}^{-1} \text{ K}^{-1}, \quad (1)$$

where $V_{\text{m,gas}}$ and $V_{\text{m,liquid}}$ are the molar volume of the solute in the gas phase and solvent, respectively. The detailed information about Equation 1 has been given in Wertz.^[64] This equation for the solute in thf can be written as follows (Equation 2).

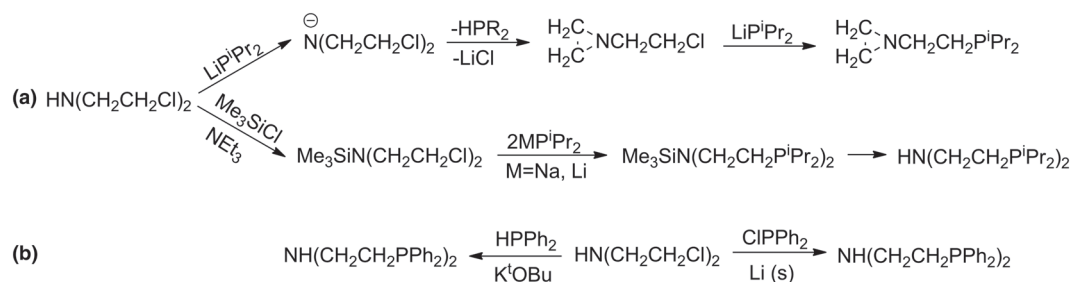
$$\text{THF: } \Delta S_{\text{solvation}} (\text{cal mol}^{-1} \text{ K}^{-1}) = -11.301 - 0.208 (S^\circ - 11.301) + 7.98. \quad (2)$$

3 | RESULT AND DISCUSSION

3.1 | Synthesis and characterization

In contrast to the usual synthetic methods, which are based on time-consuming and costly amine protection (Scheme 3a), this study avoids this by using LiPPh_2 which has low basicity and high nucleophilicity thereby preventing the aziridine formation (Scheme 3).^[38,65,66]

The $\text{P}^{\wedge}\text{N}^{\wedge}\text{P}$ ligand was then characterized by ^1H NMR, ^{31}P NMR, FT-IR, UV-vis, and single-crystal X-ray diffraction. The calculated and experimental FT-IR



SCHEME 3 Synthetic procedures of bis[(2-dialkyl/arylphosphino)ethyl]amine ($\text{P}^i\text{N}^i\text{P}^i$)

spectra of the Ni complex and the ligand are shown in Figure S1. In the ligand, the band at 3425 cm^{-1} is related to amine functional group. CH (aromatic) vibrational modes appear at 3070 cm^{-1} . The bands at 2850 and 1400 cm^{-1} relate to $-\text{CH}$ (aliphatic) and $\text{C}=\text{C}$ stretching modes, respectively. Also, the complex FT-IR spectrum of the complex shows vibrational bands of the ligand with a few changes in intensities and band positions.

The ^1H NMR spectrum of the ligand displays a signal at 9.8 ppm for NH_2^+ hydrogens. In addition, two signals were observed at 2.8 and 2.4 ppm assigned to the methylene groups. In the ^{31}P NMR spectrum of the ligand showed a major signal can be seen at -21.5 ppm , which is consistent with reported values^[62,66,67] and a minor one at 34.5 ppm for the oxidized product.^[62] The ^1H , ^{13}C , and ^{31}P NMR of $[\text{NiCl}(\text{P}^i\text{N}^i\text{P}^i)]\text{Cl}$ are shown in Figures S2–S4. ^1H NMR resonances of the complex also displayed two multiplets, 2.14 – 2.49 and 2.74 – 3.39 , related to two chemically nonequivalent CH_2 groups from the ligand. The amine signal was observed at a higher value (10.44 ppm) in the complex compared to the ligand (9.8 ppm) (Figure S2). The ^{13}C NMR spectrum showed

two signals at δ , 28.9 and 51.6 ppm , for two CH_2 fragments. The observed signals in the range of 129 to 135 ppm are assigned to aromatic carbons (Figure S3). A single resonance at $\delta = 28\text{ ppm}$ was observed in the ^{31}P $\{^1\text{H}\}$ NMR spectrum of the complex whereas the ligand signal positioned at -21 ppm , which may suggest formation of the pincer complex (Figure S4). This value is in accordance with similar complexes; for example, Tamizmani and Sivasankar had synthesized $[\text{PN}(\text{H})\text{P}^{\text{Ph}}\text{NiCl}]$ with P chemical shift at 27.6 ppm .^[68]

UV–vis spectra of the ligand and the Ni complex were recorded in EtOH. The calculated and experimental absorption spectra have been shown in Figure 1, and the contribution of molecular orbitals in electronic transmissions are shown in Tables 1 and 2. The experimental spectrum of the ligand showed two bands at 230 and 248 nm , respectively. Upon formation of the Ni complex, as well as a band at 224 nm , three additional bands emerge at 264 , 343 , and 471 nm , respectively. There is a relatively good agreement between the calculated and experimental spectra. So DFT calculation helped to identify the type of transitions for each band.

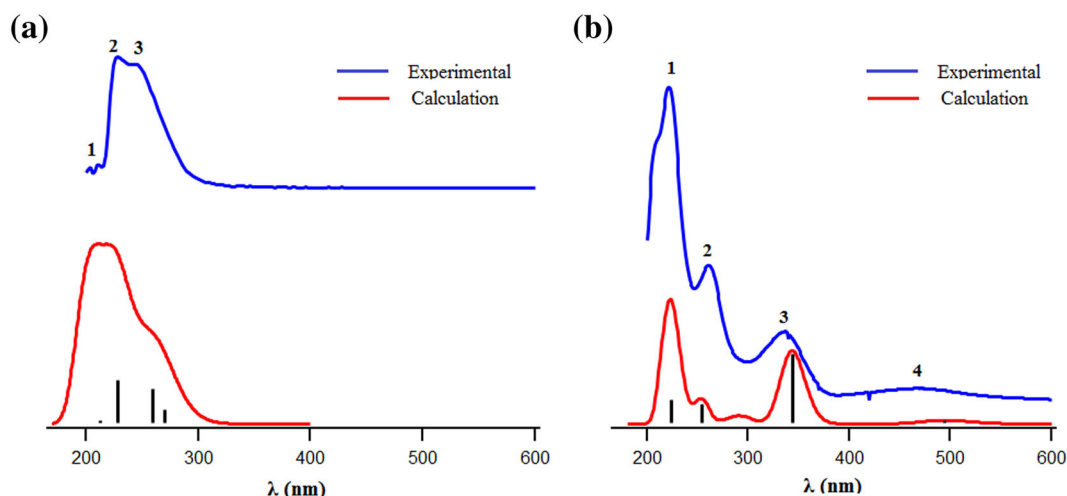
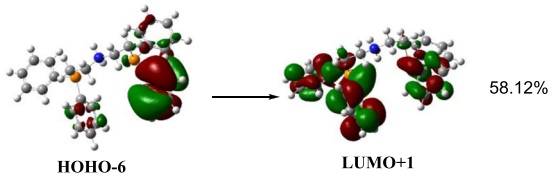
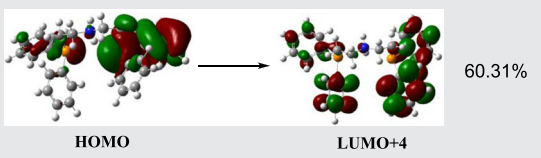
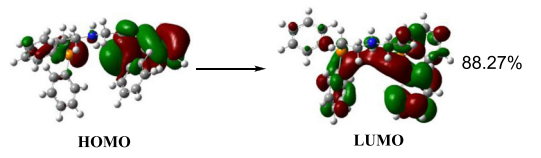
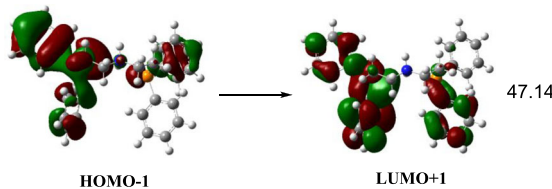
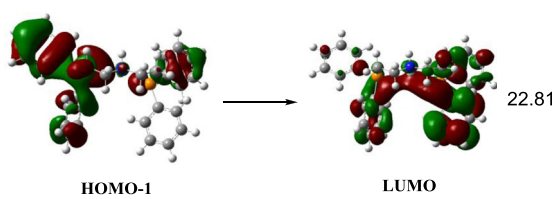


FIGURE 1 Density functional theory (DFT) calculation and experimental electronic spectra of (a) $\text{P}^i\text{N}^i\text{P}^i\cdot\text{HCl}$ (ligand) and (b) $[\text{Ni}(\text{P}^i\text{N}^i\text{P}^i)\text{Cl}]\text{Cl}$ (complex)

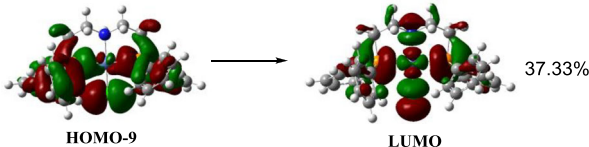
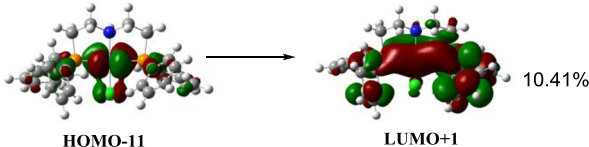
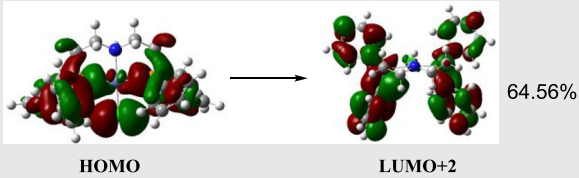
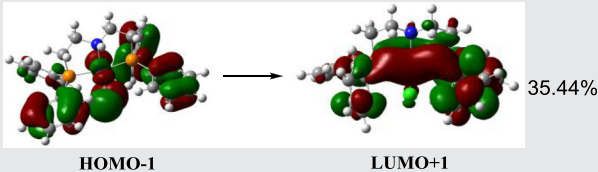
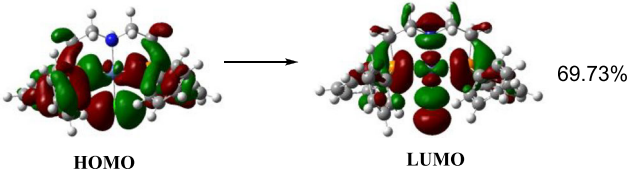
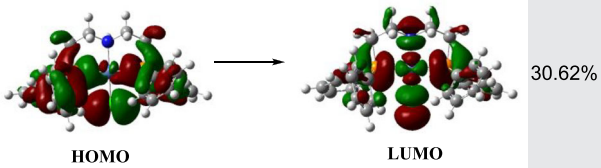
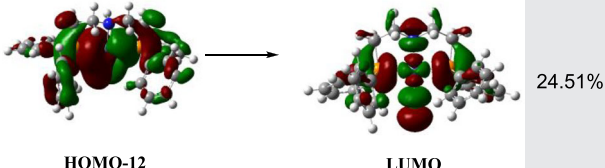
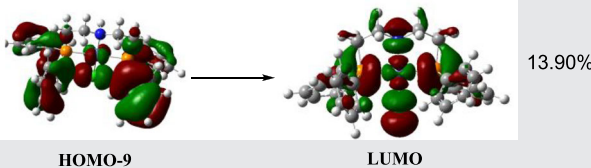
TABLE 1 Experimental and calculated electronic transitions by Time-Dependent DFT/Polarizable Continuum Model (TDDFT/PCM) method of P⁺N⁺P.HCl (ligand) in ethanol

Transition number	$E_{\text{excitation}}$ (eV)	λ_{expt} (nm)	λ_{calc} (nm)	Key transitions
1	5.81	210	213	
2	5.43	232	228	
3	4.59	250	269	
	4.77		259	
				

In the calculated ligand spectrum, the band at 259 nm originated from HOMO - 1 \rightarrow LUMO and HOMO - 1 \rightarrow LUMO + 1. The HOMO - 1 \rightarrow LUMO is related to the excitation of an electron from the lone pair (Lp) of P atom and π (C—C) of the phenyl ring in part A of the ligand to the π^* (C—C) of the phenyl ring in part B of the ligand (both parts A and B are shown in Figure 2). Similarly, the HOMO - 1 \rightarrow LUMO + 1 is the excitation of Lp of P atom and π (C—C) of the phenyl ring in part A of the ligand to π^* (C—C) of the phenyl ring in part A of the ligand. It can be said that these two transitions are $n \rightarrow \pi^*$ transitions. The band at 269 nm originates from the HOMO \rightarrow LUMO. The HOMO \rightarrow LUMO is also related to the excitation of an electron from the lone pair (Lp) of P atom and π (C—C) of the phenyl ring in part B of the ligand to the π^* (C—C) of the phenyl ring in part B of

the ligand. The band located at 228 nm is due to two orbital excitation, including HOMO \rightarrow LUMO + 4. The HOMO \rightarrow LUMO + 4 excitation is due to the electron excitation from Lp(P) and π (C—C) of phenyl rings in part B of the ligand to π^* (C—C) of the phenyl ring in the same part of the ligand. The band located at 213 nm was due to orbital excitation, including HOMO - 6 \rightarrow LUMO + 1. The HOMO - 6 \rightarrow LUMO + 1 excitation is due to the electron excitation from π (C—C) of the phenyl ring in part B of the ligand to π^* of C—C of the phenyl ring in part A of the ligand. In the absorption spectrum of complex, the absorption band located at 494 nm has the contribution of HOMO \rightarrow LUMO (30.6%) assigned to the excitation of Lp of Cl and σ of P—Ni and P—C bonds to σ^* of Ni—Cl and Ni—P bonds. Other orbital transitions of these absorption bands are assigned to

TABLE 2 Experimental and calculated electronic transitions by TDDFT/PCM method of $[\text{Ni}(\text{P}^{\wedge}\text{N}^{\wedge}\text{P})\text{Cl}]\text{Cl}$ in ethanol

Transition number	$E_{\text{excitation}}$ (eV)	λ_{expt} (nm)	λ_{calc} (nm)	Key transitions
1	5.54	224	223.95	 HOMO-9 → LUMO 37.33%  HOMO-11 → LUMO+1 10.41%
2	4.87	264	254.71	 HOMO → LUMO+2 64.56%  HOMO-1 → LUMO+1 35.44%
3	3.61	343	343.47	 HOMO → LUMO 69.73%
3	2.51	471	494.55	 HOMO → LUMO 30.62%  HOMO-12 → LUMO 24.51%  HOMO-9 → LUMO 13.90%

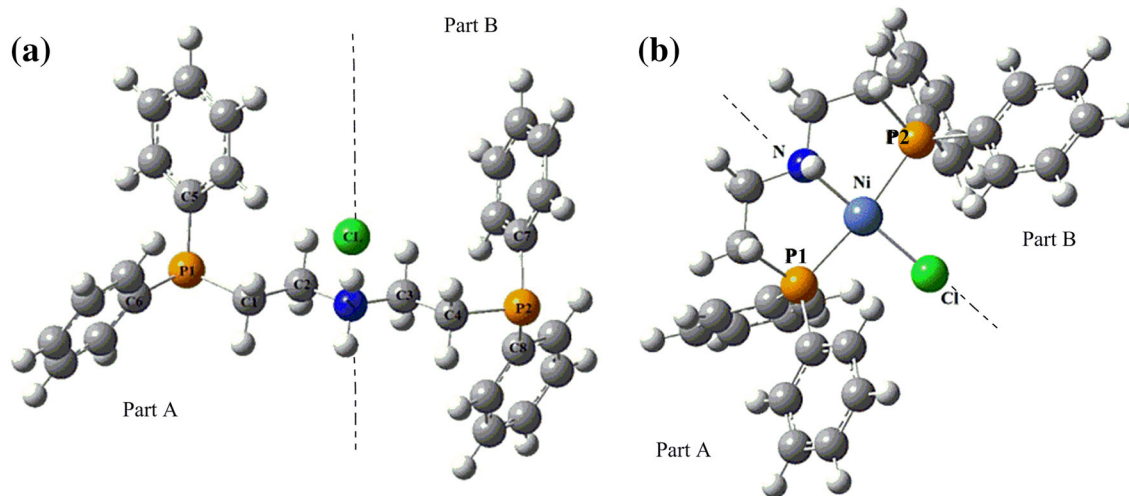


FIGURE 2 The optimized structures of (a) $P^N P.HCl$ and (b) $[Ni(P^N P)Cl]Cl$ in the gas phase

HOMO – 12 \rightarrow LUMO and HOMO – 9 \rightarrow LUMO. The HOMO – 12 \rightarrow LUMO is related to the excitation of Lp electrons of Ni, σ P1–C, and σ P2–Ni to σ^* Ni–Cl and σ^* P–Ni. The HOMO – 9 \rightarrow LUMO is related to the excitation of $\pi(C-C)$ of the phenyl ring of part A of the ligand to σ^* Ni–Cl and σ^* P–Ni. The absorption band located at 264 nm is due to two orbital excitations, including HOMO \rightarrow LUMO + 2 and HOMO – 1 \rightarrow LUMO + 1. The HOMO \rightarrow LUMO + 2 is related to the excitation of Lp of Cl, σ P–Ni, and P–C to $\pi^*(C-C)$ of the phenyl ring of part A of the ligand. The HOMO – 1 \rightarrow LUMO + 1 is assigned to the excitation of an electron from the Lp of Cl and Ni atoms and $\pi(C-C)$ of the phenyl ring of part A of the ligand to the $\pi^*(C-C)$ of the phenyl ring of part B of the ligand. The highest intensity band at 223 nm in the spectrum of the complex is assigned to

HOMO – 9 \rightarrow LUMO and HOMO – 11 \rightarrow LUMO + 1 orbital excitations. The HOMO – 9 \rightarrow LUMO is related to the excitation of an electron from $\pi(C-C)$ of the phenyl rings of part A of ligand to $\pi^*(C-C)$ of the phenyl ring in the same part. The HOMO – 11 \rightarrow LUMO + 1 is related to the excitation of Lp electrons of Ni to $\pi^*(C-C)$ phenyl ring in part B of the ligand (Figure 2).

The X-ray structures and crystal data of the ligand and the complex are shown in Figure 3 and Table 3, respectively. This complex was first synthesized by Walther et al. in 1999 and crystallized in thf in a triclinic system with $a = 11.745(1)$, $b = 12.148(1)$, and $c = 14.129(3)$ Å lattice parameters.^[69] In this study, the single crystal of the complex was obtained in ethanol with a monoclinic crystal system with $a = 15.4956(4)$, $b = 9.1535(3)$, and $c = 23.7002(6)$ Å lattice parameters. The ligand and

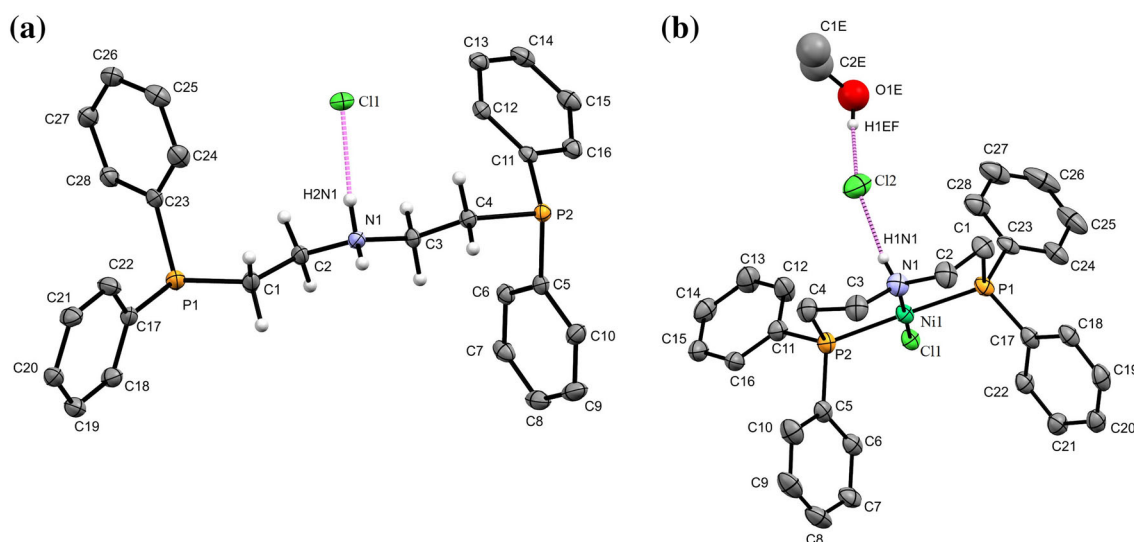


FIGURE 3 ORTEP diagram of (a) $P^N P.HCl$ and (b) $[Ni(P^N P)Cl]Cl.EtOH$ (some hydrogens are not shown for more clarity)

TABLE 3 Crystal data and structural refinement

Crystal data	P [^] N [^] P.HCl	[Ni(P [^] N [^] P)Cl]Cl.EtOH
Empirical formula	C ₂₈ H ₃₀ ClNP ₂	C ₃₀ H ₃₅ Cl ₂ NNiOP ₂
Formula weight	477.92	617.14
Temperature (K)	133(2)	133(2)
Wavelength (Å)	0.71073	0.71073
Crystal system	Monoclinic	Monoclinic
Space group	<i>P</i> 2 ₁ / <i>c</i>	<i>P</i> 2 ₁ / <i>c</i>
<i>a</i> (Å)	10.1149(3)	15.4956(4)
<i>b</i> (Å)	26.7526(7)	9.1535(3)
<i>c</i> (Å)	10.2717(3)	23.7002(6)
α (°)	90	90
β (°)	114.210(1)	103.971(2)
γ (°)	90	90
<i>V</i> (Å ³)	2535.06(12)	3262.17(16)
<i>Z</i>	4	4
Density	1.252	1.257
Absorption coefficient (mm ⁻¹)	0.293	0.879
<i>F</i> (000)	1008	1262
Crystal size (mm)	0.122 × 0.112 × 0.108	0.132 × 0.122 × 0.105
θ Range for data	2.21–27.46	1.952–27.48
Reflection collected	17,501	38,930
Independent reflection	5747 (<i>R</i> _{int} = 0.0641)	7439 (<i>R</i> _{int} = 0.0641)
Max. and min. transmission	0.7456 and 0.6576	0.7456 and 0.6314
Data/restraints/parameters	5747/0/297	7439/18/3351
Goodness-of-fit <i>F</i> ²	1.076	1.104
Final <i>R</i> indices [<i>I</i> > 2σ(<i>I</i>)]	<i>R</i> ₁ = 0.0607, <i>wR</i> ₂ = 0.1401	<i>R</i> ₁ = 0.0922, <i>wR</i> ₂ = 0.2390
<i>R</i> indices (all data)	<i>R</i> ₁ = 0.0760, <i>wR</i> ₂ = 0.1486	<i>R</i> ₁ = 0.1230, <i>wR</i> ₂ = 0.2663

complex were crystallized in monoclinic *P*2₁/*c* space groups. The molecular structure of the complex contains a distorted four-coordinated square-planar geometry. The Ni(II) coordination sphere includes one tridentate ligand that forms two five-member rings and one Cl atom at *trans* position to N atom of PNP ligand (Figure 3). The P1–Ni–P2 angle is 170.86(6)°, and the deviation from the ideal value for square-planar coordination is due to the steric constraints of the chelating ligand. The length of the bonds for Ni–P1, Ni–P2, and Ni–N are 2.1927(16), 2.1930(16), and 1.934(5) Å, respectively, which indicates that the phosphorus atoms are located at the same distance from the central metal. Four coordinate geometric parameter (FCGP) was also calculated for the geometry determination of the pincer complex. For tetrahedral and square planar geometry, the expected FCGPs are 100 and –40, respectively.^[70] For [Ni(P[^]N[^]P)

Cl]Cl.EtOH the obtained FCGP parameters is –43, which suggest a distorted square-planar geometry.

3.2 | Electrocatalytic hydrogen ion reduction

Although it is already well-known, no known studies into the use of [Ni(P[^]N[^]P)Cl]Cl for electrocatalytic hydrogen evolution have been carried out. Therefore, the electrochemical analysis was performed in a 0.1 M NBu₄BF₄ acetonitrile solution under an Ar atmosphere containing 1 mM [Ni(P[^]N[^]P)Cl]Cl.EtOH. In CVs of 1 mM [Ni(P[^]N[^]P)Cl]Cl.EtOH at different scan rates (30, 50, 100, and 150 mV s⁻¹) reduction peaks could be observed approximately –0.5 V versus NHE, which were subsequently assigned to a Ni^{II}/Ni^I couple (Figure 4).

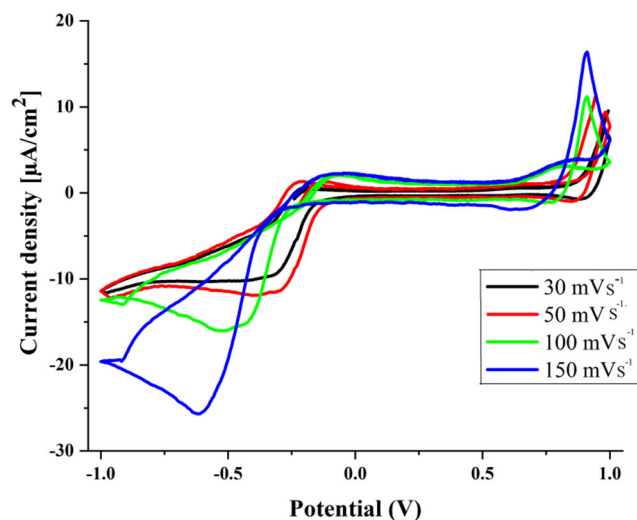


FIGURE 4 Cyclic voltammograms of 1 mM $[\text{Ni}(\text{P}^{\text{N}}\text{P})\text{Cl}]\text{Cl}$ in EtOH in 0.1 M NBu_4BF_4 in acetonitrile solution at different scan rates

As electrochemical methods are helpful in determining the potential of hydrogen evolution by Ni pincer complexes, we investigated the electrocatalytic hydrogen ion reduction activity of $[\text{Ni}(\text{P}^{\text{N}}\text{P})\text{Cl}]\text{Cl}\cdot\text{EtOH}$ in the presence of 1 M HCl in anhydrous acetonitrile. As shown in Figure 5, the incremental addition of HCl solution (15, 65, 80, and 100 μL) renders the reduction wave of $\text{Ni}^{2+}/\text{Ni}^+$ couple with an accompanying increase in the current. This behavior is characteristic of electrocatalytic hydrogen ion reduction and suggests hydrogen evolution by the $[\text{Ni}(\text{P}^{\text{N}}\text{P})\text{Cl}]\text{Cl}\cdot\text{EtOH}$ catalyst. Figure 6 shows stability test on $[\text{Ni}(\text{P}^{\text{N}}\text{P})\text{Cl}]\text{Cl}\cdot\text{EtOH}$, which was

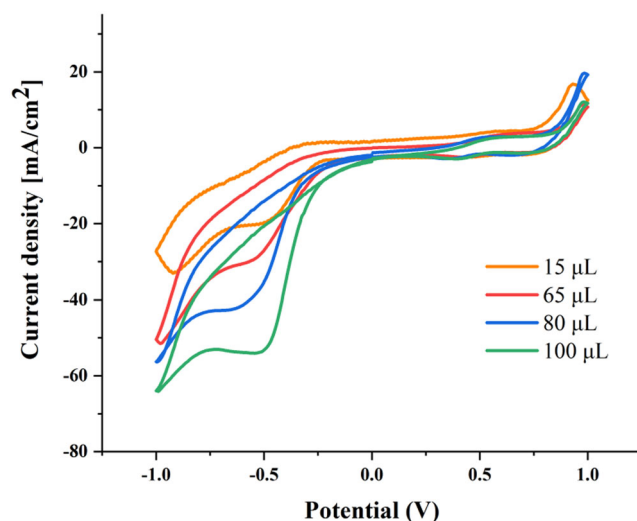


FIGURE 5 Cyclic voltammograms of 1 mM solutions of $[\text{Ni}(\text{P}^{\text{N}}\text{P})\text{Cl}]\text{Cl}\cdot\text{EtOH}$ with various amounts of HCl in 0.1 M NBu_4BF_4 in acetonitrile solution at a scan rate of 0.1 V s^{-1}

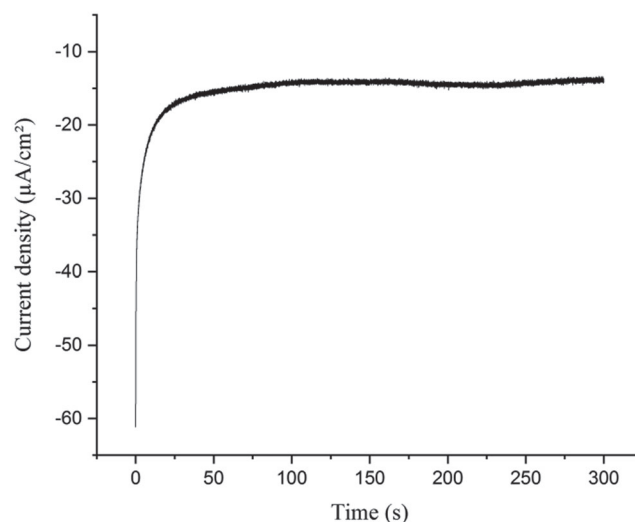


FIGURE 6 The chronoamperometric curve of $[\text{Ni}(\text{P}^{\text{N}}\text{P})\text{Cl}]\text{Cl}\cdot\text{EtOH}$

evaluated by the chronoamperometry (i-t) technique. The data suggests that this complex is stable at a current density of -16 mA cm^{-2} and continues this sustainability for 300 s in the presence of 100- μL HCl.

3.3 | In vitro cytotoxicity

Cytotoxic effects of $[\text{Ni}(\text{P}^{\text{N}}\text{P})\text{Cl}]\text{Cl}\cdot\text{EtOH}$ on MCF7 and HT29 cancer cells were determined after 1 and 2 days of culture via MTT assay. Three different concentrations of $[\text{Ni}(\text{P}^{\text{N}}\text{P})\text{Cl}]\text{Cl}\cdot\text{EtOH}$ (50, 100, and 200 μM) were prepared and used for cell viability studies. Cell viability in the presence of complex (50, 100, and 200 μM) treated for 1 day with MCF7 cancer cells was seen to increase from 89.96 to 127.59 (% control). Moreover, the relative cell viability was enhanced from the least concentration (50 μM) to the highest (200 μM). The proliferation of MCF7 cells was reduced in the second day for 100 and 200 μM to 89.47 and 105.55 (% control) (Figure 7).

For HT29 cancer cells, the MTT assay of the complex after 1 day shows that the cell viability at 100 μM has the highest value (83.10%), and 200 μM has the lowest one (71.26%). After 2 days, the cell viability dose not display any significant changes for 50 and 100 μM of the complex whereas at higher concentration i.e. 200 μM , it undergoes a decrease. The proliferation of cells cultured on the 200 μM was seen to decrease from 71.26 (% control) (after 1 day) to 37.80 (% control) (after 2 days) (Figure 8). It could be therefore concluded that the viability of the two cancer cells in the presence of $[\text{Ni}(\text{P}^{\text{N}}\text{P})\text{Cl}]\text{Cl}\cdot\text{EtOH}$ depends on culture time and concentration of the complex.

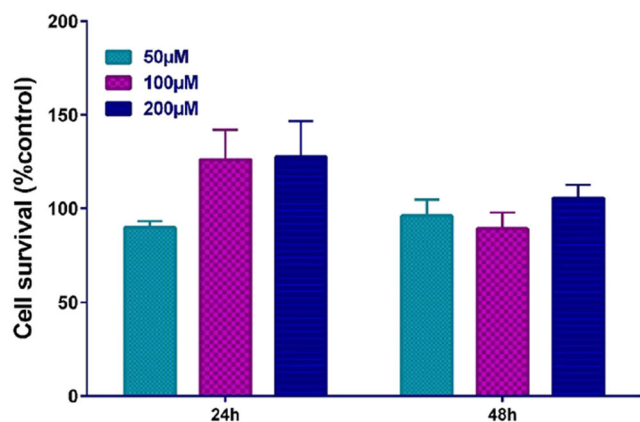


FIGURE 7 A comparative plot of the cell viability of MCF7 in the presence of 50, 100, and 200 μM of $[\text{Ni}(\text{P}^{\wedge}\text{N}^{\wedge}\text{P})\text{Cl}]\text{Cl.EtOH}$ after 1 and 2 days

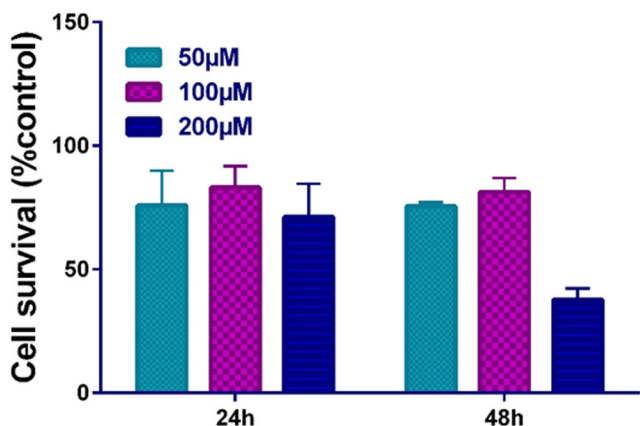


FIGURE 8 A comparative plot of the cell viability of HT29 in the presence of 50, 100, and 200 μM of $[\text{Ni}(\text{P}^{\wedge}\text{N}^{\wedge}\text{P})\text{Cl}]\text{Cl.EtOH}$ after 1 and 2 days

The results from the cytotoxicity tests show IC_{50} values of 58.2 μM (1 day) and 193.2 (2 days), for $[\text{Ni}(\text{P}^{\wedge}\text{N}^{\wedge}\text{P})\text{Cl}]\text{Cl.EtOH}$ in the presence of MCF7 cells of which the former value is lower than that of *cis*-platin (Table 4). Using HT29 cells instead the same tests reveal IC_{50} values of 205.3 and 79.0 μM after 1 and 2 days, respectively, which are higher than *cis*-platin (Table 4). These results suggest that the pincer complex displays better cytotoxic activities than *cis*-platin against MCF7 cancer cells after 1 day.

TABLE 4 IC_{50} values for $[\text{Ni}(\text{P}^{\wedge}\text{N}^{\wedge}\text{P})\text{Cl}]\text{Cl.EtOH}$ and *cis*-platin in the presence of MCF7 and HT29 cell lines

Sample	Cancer cell	IC_{50} (μM) 1 day (3 points)	IC_{50} (μM) 2 days (3 points)
<i>cis</i> -Platin	MCF7	67.0	111.9
	HT29	101.8	23.3
$[\text{Ni}(\text{P}^{\wedge}\text{N}^{\wedge}\text{P})\text{Cl}]\text{Cl.EtOH}$	MCF7	58.2	193.2
	HT29	205.3	79.0

3.4 | Computational results

The structures of the pincer ligand and its corresponding nickel complex obtained from the single-crystal X-ray diffraction were compared with their optimized structures, with the latter shown in Figure 2. The experimental and computational selected bond lengths and angles for the ligand and the complex are also listed in Tables 5 and 6, respectively.

From the tabulated data it can be surmised that there is a good agreement between the calculated values in the gas phase and the obtained experimental values in the solid state, for both ligand and complex with any structural differences between the free and complexed ligand being negligible. The experimental and theoretical values of bond lengths and bond angles for the ligand were compared and are shown in Table 5. The kinetics and thermodynamics of the ligand synthesis with *iso*-propyl substituents on the P atoms were already previously investigated in detail,^[30] and we just briefly studied the theoretical calculation of the phenyl substituents. The optimized structures of the TSs related to the reaction of lithium diphenylphosphanide (LiPPh_2) reaction with bis (2-chloroethyl)amine are shown in Figure 9. The calculations show that activation free energy (ΔG^\ddagger) in the absence of solvent is 31.05 kcal mol^{-1} (rate constant (k) = $1.05 \times 10^{-10} \text{ s}^{-1}$) but, when the electrostatic fields of thf were considered as a solvent, the activation free energy changed to 20.14 kcal mol^{-1} (rate constant (k) = $6.62 \times 10^{-5} \text{ s}^{-1}$). It was then found that the synthesis of the pincer ligand in the gas phase was undesirable, whereas in the thf, the reaction became more thermodynamically favorable. The calculated ΔG values for the $\text{P}^{\wedge}\text{N}^{\wedge}\text{P}$ ligand synthesis in the gas phase and thf for the first step were 121.70 and $-25.34 \text{ kcal mol}^{-1}$, respectively.

3.5 | Proposed electrocatalytic and thermodynamic cycle

Previously, various nickel complexes have been synthesized and used as hydrogen ion reduction electrocatalysts for hydrogen evolution. For example, Goh et al. reported bis(cyclopentadienyl)nickel(II)- μ -thiolato complexes as

	Bond lengths (Å)			Bond angles (°)	
	Exp.	Comp.		Exp.	Comp.
P(1)-C(1)	1.845(3)	1.853	C(2)-N(1)-C(3)	112.9(2)	115.19
C(1)-C(2)	1.527(4)	1.521	C(3)-C(4)-P(2)	117.37(18)	117.28
C(2)-N(1)	1.489(4)	1.489	C(5)-P(1)-C(1)	102.01(12)	98.62
N(1)-H(1)	0.86(4)	1.025	C(6)-P(1)-C(1)	101.64(14)	102.78
C(3)-C(4)	1.517(4)	1.521	C(4)-P(2)-C(8)	103.44(12)	101.48
C(4)-P(2)	1.851(3)	1.856	C(4)-P(2)-C(7)	100.09(12)	103.12

TABLE 5 Experimental and computational values of selected bond lengths and bond angles of P^{AN}P.HCl

	Bond length (Å)			Bond angles (°)	
	Exp.	Comp.		Exp.	Comp.
Ni(1)-N(1)	1.934(5)	1.976	N(1)-Ni(1)-Cl(1)	174.83(18)	174.67
Ni(1)-Cl(1)	2.1588(14)	2.1793	N(1)-Ni(1)-P(1)	86.16(18)	87.26
Ni(1)-P(1)	2.1935(16)	2.2481	Cl(1)-Ni(1)-P(1)	93.80(6)	92.74
Ni(1)-P(2)	2.1920(16)	2.2499	N(1)-Ni(1)-P(2)	86.16(18)	87.15
N(1)-H(1 N1)	2.06(10)	1.025	P(1)-Ni(1)-P(2)	170.86(6)	170.53
N(1)-C(2)	1.497(8)	1.4896	Cl(1)-Ni(1)-P(2)	94.35(6)	93.54

TABLE 6 Experimental and computational values of selected bond lengths and bond angles of [Ni(P^{AN}P)Cl]Cl

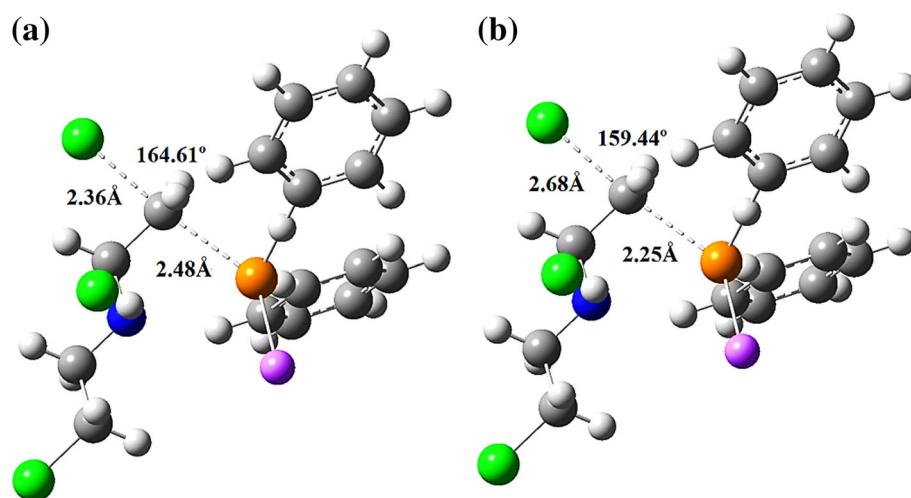


FIGURE 9 TS structures related to the reaction of bis(2-chloroethyl)amine with lithium diphenylphosphanide (LiPPH₂) (a) in the gas phase and (b) in tetrahydrofuran (thf), which considered as a polarized continuum solvent

hydrogen ion reduction electrocatalysts. The proposed reaction pathways for reducing two hydrogen ions to generate an dihydrogen molecule involve four steps in the form of either chemical (C) or electrochemical (E) reactions.^[71] In another study, Hong et al. synthesized high-spin Ni(II) complexes with S₂N₂ ligands. The proposed electrocatalytic mechanism involves the stepwise reduction of Ni(II) by two electrons to form [LNi⁰]⁰ in acetonitrile.^[72] A mechanism for the hydrogen ion reduction using the PCP pincer complex has been reported by Luca et al.^[42] A similar mechanism has been considered

for the hydrogen ion reduction using the synthesized complex in this work with some modifications (see Figure 10). The optimized structures of the complex at each step of the cycle are also shown in Figure 10. The first step is one-electron reduction of [1-Cl]⁺ complex to [2-Cl]⁰ which is a spontaneous reaction ($\Delta G = -92.33$ kcal mol⁻¹; step A, Figure 10). In the next step, the [2-Cl]⁰ is protonated to form Ni^{III} hydride [1-H]⁺ ($\Delta G = -143.27$ kcal mol⁻¹, step B). In step C, the subsequent Ni^{III} hydride [1-H]⁺ is reduced by one electron to give Ni^{II} hydride, [1-H]⁰. To complete the cycle,

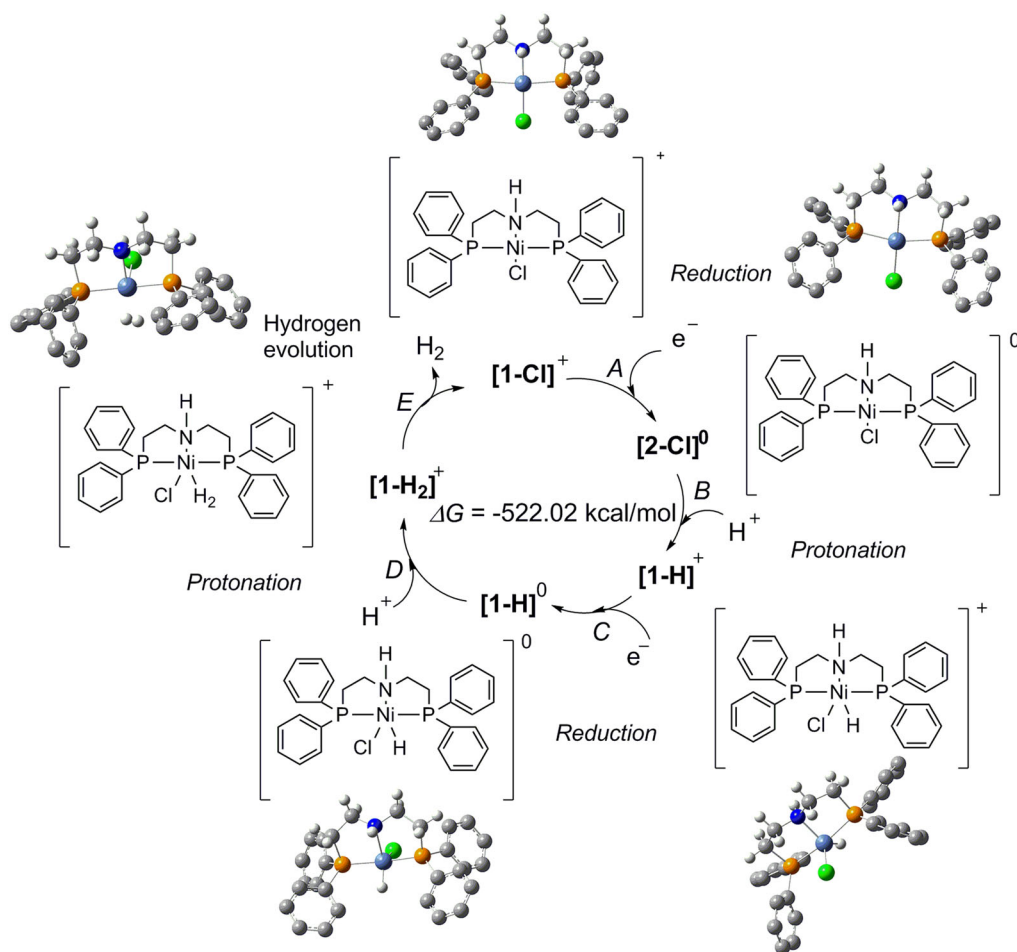


FIGURE 10 Mechanism of hydrogen evolution by $[\text{Ni}(\text{P}^{\wedge}\text{N}^{\wedge}\text{P})\text{Cl}]\text{Cl}.\text{EtOH}$

with protonation of $[1-\text{H}]^0$, the $[1-\text{H}_2]^+$ complex was formed as an intermediate ($\Delta G = -162.25 \text{ kcal mol}^{-1}$, step D). Finally, the $[1-\text{H}_2]^+$ complex loses one H_2 molecule to revitalize the initial $[1-\text{Cl}]^+$ complex. The calculated value of ΔG° (total) for the electrocatalytic cycle is $-522.02 \text{ kcal mol}^{-1}$, which shows the cycle is thermodynamically favorable and the $[\text{NiCl}(\text{P}^{\wedge}\text{N}^{\wedge}\text{P})]\text{Cl}$ can reduce hydrogen ion to H_2 (Figure 10).

4 | CONCLUSION

The $\text{P}^{\wedge}\text{N}^{\wedge}\text{P}$ -type pincer ligand, bis[(2-diphenylphosphino)ethyl]amine, has been synthesized simply and fully characterized employing different analytical techniques. It was then used to prepare its Ni(II) complex, $[\text{Ni}(\text{P}^{\wedge}\text{N}^{\wedge}\text{P})\text{Cl}]\text{Cl}.\text{EtOH}$, which was analysed using FT-IR, UV-visible, ^1H NMR, ^{13}C NMR, and ^{31}P NMR spectroscopies, single-crystal X-ray diffraction, and CHN analyses. The molecular structure of the complex has a four-coordinated distorted nickel ion with square-planar geometry. CV studies revealed that the complex is an

efficient electrocatalyst for hydrogen evolution at the potential of the Ni(II/I) couple. The crystal structures of the ligand and the complex were determined by single-crystal X-ray diffraction. DFT calculations were performed to study the kinetics and thermodynamics of the synthetic procedure of the pincer ligand and the Ni complex. Theoretical calculations revealed that the synthesis of the ligand follows an $\text{S}_{\text{N}}2$ mechanism. Biological activity studies of $[\text{NiCl}(\text{P}^{\wedge}\text{N}^{\wedge}\text{P})]\text{Cl}$ showed that the death of cancer cells by pincer nickel complex depends on two factors: concentration and time. In this way, the highest efficiency for cancer cells' death was found for MCF7 cancer cells in low concentration (50 μl) and less time (24 h) thus suggesting that the complex is considerably more cytotoxic than *cis*-platin against MCF7 cancer cells within a 24-hour period.

ACKNOWLEDGMENTS

This research was supported by the Iran National Science Foundation (INSF) (Grant No. 94005007) and Research Affairs Division of Isfahan University of Technology (IUT), Isfahan, I. R. Iran.

AUTHOR CONTRIBUTIONS

Gholamhossein Mohammadnezhad: Conceptualization; data curation; funding acquisition; investigation; project administration. **Saeed Abad:** Conceptualization; data curation; formal analysis; investigation; software; validation. **Hossein Farrokhpour:** Conceptualization; data curation; supervision. **Helmar Görls:** Data curation; software; validation. **Winfried Plass:** Funding acquisition; resources.


SUPPORTING INFORMATION AVAILABLE

Crystallographic data (excluding structure factors) has been deposited with the Cambridge Crystallographic Data Centre as supplementary publication CCDC-2020952 for P^N^P.HCl, and CCDC-2020953 for [Ni (P^N^P)Cl].EtOH. Copies of the data can be obtained free of charge on application to CCDC, 12 Union Road, Cambridge CB2 1EZ, UK (Email: deposit@ccdc.cam.ac.uk). Additional supporting information may be found online in the Supporting Information.

DATA AVAILABILITY STATEMENT

Research data are not shared.

ORCID

Gholamhossein Mohammadnezhad  <https://orcid.org/0000-0003-1765-8063>

Winfried Plass  <https://orcid.org/0000-0003-3473-9682>

REFERENCES

- [1] C. Gunanathan, D. Milstein, *Chem. Rev.* **2014**, *114*, 12024.
- [2] P. Daw, S. Chakraborty, G. Leitus, Y. Diskin-Posner, Y. Ben-David, D. Milstein, *ACS Catal.* **2017**, *7*, 2500.
- [3] P. M. Schroder, T. F. Spilker, W. Luu, J. B. Updegraff III, M. L. Kwan, P. R. Challen, J. D. Protasiewicz, *Inorg. Chem. Commun.* **2009**, *12*, 1171.
- [4] A. K. W. Chan, D. Wu, K. M. C. Wong, V. W. W. Yam, *Inorg. Chem.* **2016**, *55*, 3685.
- [5] S. Menuel, E. Bertaut, E. Monflier, F. Hapiot, *Dalton Trans.* **2015**, *44*, 13504.
- [6] P. Zabierowski, D. Matoga, W. Nitek, *RSC Adv.* **2015**, *5*, 25911.
- [7] M. Zhang, P. Hu, J. Zhou, G. Wu, S. Huang, W. Su, *Org. Lett.* **2013**, *15*, 1718.
- [8] K. Li, T. Zou, Y. Chen, X. Guan, C. M. Che, *Chem. – Eur. J.* **2015**, *21*, 7441.
- [9] B. Boff, C. Gaidon, M. Pfeffer, *Inorg. Chem.* **2013**, *52*, 2705.
- [10] N. Cutillas, G. S. Yellol, C. de Haro, C. Vicente, V. Rodríguez, J. Ruiz, *Coord. Chem. Rev.* **2013**, *257*, 2784.
- [11] S. Ramírez-Rave, M. T. Ramírez-Apan, H. Tlahuext, D. Morales-Morales, R. A. Toscano, J. M. Grévy, *J. Organomet. Chem.* **2016**, *814*, 16.
- [12] B. Bertrand, A. Casini, *Dalton Trans.* **2014**, *43*, 4209.
- [13] B. K. Tate, C. M. Wyss, J. Bacsá, K. Kluge, *Chem. Sci.* **2013**, *4*, 3068.
- [14] H. Tavallali, G. Deilamy-Rad, A. Moaddeli, K. Asghari, *Sens. Actuatur B-Chem.* **2017**, *244*, 1121.
- [15] S. Sobhani, A. Habibollahi, Z. Zeraatkar, *Org. Process Res. Dev.* **2019**, *23*, 1321.
- [16] J. P. Cloutier, B. Vabre, B. Moungang-Soume, D. Zargarian, *Organometallics* **2014**, *34*, 133.
- [17] A. R. Chianese, M. J. Drance, K. H. Jensen, S. P. McCollom, N. Yusufova, S. E. Shaner, J. A. Tendler, *Organometallics* **2014**, *33*, 457.
- [18] F. R. Negreiros, M. F. Camellone, S. Fabris, *J. Phys. Chem. C* **2015**, *119*, 21567.
- [19] S. Chakraborty, P. O. Lagaditis, M. Förster, E. A. Bielinski, N. Hazari, M. C. Holthausen, S. Schneider, *ACS Catal.* **2014**, *4*, 3994.
- [20] M. Nielsen, E. Alberico, W. Baumann, H. J. Drexler, H. Junge, S. Gladiali, M. Beller, *Nature* **2013**, *495*, 85.
- [21] A. Staubitz, M. E. Sloan, A. P. Robertson, A. Friedrich, S. Schneider, P. J. Gates, I. Manners, *J. Am. Chem. Soc.* **2010**, *132*, 13332.
- [22] M. Käb, A. Friedrich, M. Drees, S. Schneider, *Angew. Chem., Int. Ed.* **2009**, *48*, 905.
- [23] A. Glueer, S. Schneider, *J. Org. Chem.* **2018**, *861*, 159.
- [24] S. Schneider, J. Meiners, B. Askevold, *Eur. J. Inorg. Chem.* **2012**, *2012*, 412.
- [25] G. Van Koten, *Pure Appl. Chem.* **1989**, *61*, 1681.
- [26] T. W. Lyons, D. Bezier, M. Brookhart, *Organometallics* **2015**, *34*, 4058.
- [27] W. Leis, H. A. Mayer, W. C. Kaska, *Coord. Chem. Rev.* **2008**, *252*, 1787.
- [28] A. Plikhta, A. Pöthig, E. Herdtweck, B. Rieger, *Inorg. Chem.* **2015**, *54*, 9517.
- [29] G. Zhu, L. Wang, H. Sun, X. Li, *RSC Adv.* **2015**, *5*, 19402.
- [30] G. Mohammadnezhad, S. Abad, H. Farrokhpour, *J. Struct. Chem.* **2019**, *60*, 1735.
- [31] P. Eduardo, R. H. Crabtree, *Coord. Chem. Rev.* **2004**, *248*, 2239.
- [32] M. Gupta, C. Hagen, R. J. Flesher, W. C. Kaska, C. M. Jensen, *Chem. Commun.* **1996**, *17*, 2083.
- [33] A. J. Holmes, P. J. Rayner, M. J. Cowley, G. G. Green, A. C. Whitwood, S. B. Duckett, *Dalton Trans.* **2015**, *44*, 1077.
- [34] T. J. Korstanje, M. Lutz, J. T. Jastrzebski, R. J. Klein Gebbink, *Organometallics* **2014**, *33*, 2201.
- [35] W. C. Shih, O. V. Ozerov, *Organometallics* **2015**, *34*, 4591.
- [36] G. Mohammadnezhad, S. Abad, H. Farrokhpour, *Struct. Chem.* **2018**, *29*, 81.
- [37] M. D. Fryzuk, *Can. J. Chem.* **1992**, *72*, 2839.
- [38] A. A. Danopoulos, P. G. Edwards, *Polyhedron* **1989**, *8*, 1339.
- [39] C. Bornschein, S. Werkmeister, B. Wendt, H. Jiao, E. Alberico, W. Baumann, M. Beller, *Nat. Commun.* **2014**, *5*, 4111.
- [40] B. Chatterjee, C. Gunanathan, *Org. Lett.* **2015**, *17*, 4794.
- [41] A. Mondragón, M. Flores-Alamo, P. R. Martínez-Alanis, G. Aullón, M. Ugalde-Saldivar, I. Castillo, *Inorg. Chem.* **2014**, *54*, 619.
- [42] O. R. Luca, J. D. Blakemore, S. J. Konezny, J. M. Praetorius, T. J. Schmeier, G. B. Hunsinger, R. H. Crabtree, *Inorg. Chem.* **2012**, *51*, 8704.
- [43] U. J. Kilgore, J. A. Roberts, D. H. Pool, A. M. Appel, M. P. Stewart, M. R. DuBois, D. L. DuBois, *J. Am. Chem. Soc.* **2011**, *133*, 5861.

- [44] B. M. Lindley, R. S. Van Alten, M. Finger, F. Schendzielorz, C. Würtele, A. J. Miller, S. Schneider, *J. Am. Chem. Soc.* **2018**, *140*, 7922.
- [45] a) A. Z. El-Sonbati, M. A. Diab, S. M. Morgan, M. I. Abou-Dobara, A. A. El-Ghettany, *J. Mol. Struct.* **2020**, *1200*, 127065. b) M. A. Diab, S. G. Nozha, A. Z. El-Sonbati, M. A. El-Mogazy, S. M. Morgan, *Appl. Organomet. Chem.* **2019**, *33*, 5153. c) M. A. Diab, G. G. Mohamed, W. H. Mahmoud, A. Z. El-Sonbati, S. M. Morgan, S. Y. Abbas, *Appl. Organomet. Chem.* **2019**, *33*, 4945. d) A. Z. El-Sonbati, W. H. Mahmoud, G. G. Mohamed, M. A. Diab, S. M. Morgan, S. Y. Abbas, *Appl. Organomet. Chem.* **2019**, *33*, 5048.
- [46] a) M. A. Diab, A. Z. El-Sonbati, S. M. Morgan, M. A. El-Mogazy, *Appl. Organomet. Chem.* **2018**, *32*, 4378. b) A. Z. El-Sonbati, M. A. Diab, A. M. Eldesoky, S. M. Morgan, O. L. Salem, *Appl. Organomet. Chem.* **2019**, *33*, 4839. c) A. Z. El-Sonbati, M. A. Diab, G. G. Mohamed, M. A. Saad, S. M. Morgan, S. E. A. El-Sawy, *Appl. Organomet. Chem.* **2019**, *33*, 4973.
- [47] a) A. Z. El-Sonbati, M. A. Diab, S. M. Morgan, A. M. Eldesoky, M. Z. Balboula, *Appl. Organomet. Chem.* **2018**, *32*, 4207. b) S. M. Morgan, M. A. Diab, A. Z. El-Sonbati, *Appl. Organomet. Chem.* **2018**, *32*, 4305. c) A. Z. El-Sonbati, M. A. Diab, S. M. Morgan, H. A. Seyam, *J. Mol. Struct.* **2018**, *1154*, 354. d) S. M. Morgan, M. A. Diab, A. Z. El-Sonbati, *Appl. Organomet. Chem.* **2018**, *32*, 4281.
- [48] M. E. van der Boom, D. Milstein, *Chem. Rev.* **2003**, *103*, 1759.
- [49] N. Selander, K. J. Szabo, *Chem. Rev.* **2011**, *111*, 2048.
- [50] J. Choi, A. H. R. MacArthur, M. Brookhart, A. S. Goldman, *Chem. Rev.* **2011**, *111*, 1761.
- [51] L. J. Ming, *Med. Res. Rev.* **2003**, *23*, 697.
- [52] M. J. Clarke, F. Zhu, D. R. Frasca, *Chem. Rev.* **1999**, *99*, 2511.
- [53] E. L. Chang, C. Simmers, D. A. Knight, *Pharmaceuticals* **2010**, *3*, 1711.
- [54] M. Milenković, A. Pevec, I. Turel, M. Vujčić, M. Milenković, K. Jovanović, K. Adaila, *Eur. J. Med. Chem.* **2014**, *87*, 284.
- [55] W. L. F. Armarego, W. L. F. Armarego Christina Chai, *Purification of Laboratory Chemicals* 6th ed., Elsevier **2009**.
- [56] COLLECT, Data Collection Software, BV, Nonius, Netherlands. **1998**.
- [57] Z. Otwinowski, W. Minor, *Methods Enzymol.* **1997**, *276*, 307.
- [58] L. Krause, R. Herbst-Irmer, G. M. Sheldrick, D. Stalke, *J. Appl. Crystallogr.* **2015**, *48*, 3.
- [59] G. M. Sheldrick, *Acta Cryst.* **2008**, *A64*, 112.
- [60] G. M. Sheldrick, *Acta Cryst.* **2015**, *C71*, 3.
- [61] C. F. Macrae, P. R. Edgington, P. McCabe, E. Pidcock, G. P. Shields, R. Taylor, M. Towler, J. van de Streek, *J. Appl. Crystallogr.* **2006**, *39*, 453.
- [62] B. L. Case, J. G. Franchina, Y. S. Liu, D. E. Bergbreiter, *Chem. Ind.-New York-Marcel Dekker* **1998**, 403.
- [63] M. Frisch, G. Trucks, H. Schlegel, G. Scuseria, M. Robb, J. Cheeseman, G. Scalmani, V. Barone, B. Mennucci, G. J. I. Petersson, Wallingford Google Scholar, Gaussian 09: EM64L-G09RevB. 01, Gaussian, **2010**.
- [64] D. H. Wertz, *J. Am. Chem. Soc.* **1980**, *102*, 5316.
- [65] M. Bertoli, A. Choualeb, D. G. Gusev, A. J. Lough, Q. Major, B. Moore, *Dalton Trans.* **2011**, *40*, 8941.
- [66] M. I. García-Seijo, A. Habtemariam, D. Fernández-Anca, S. Parsons, M. E. García-Fernández, *Z. Anorg. Allg. Chem.* **2002**, *628*, 1075.
- [67] M. I. García-Seijo, A. Habtemariam, S. Parsons, R. O. Gould, M. E. García-Fernández, *New J. Chem.* **2002**, *26*, 636.
- [68] M. Tamizmani, C. Sivasankar, *J. Organomet. Chem.* **2017**, *845*, 82.
- [69] D. Walther, T. Döhler, K. Heubach, O. Klobes, B. Schweder, H. Görls, *Z. Anorg. Allg. Chem.* **1999**, *625*, 923.
- [70] A. R. Hutchison, A. Mitra, D. A. Atwood, *Main Group Chem.* **2005**, *4*, 187.
- [71] Y. X. C. Goh, H. M. Tang, W. L. J. Loke, W. Y. Fan, *Inorg. Chem.* **2019**, *58*, 12178.
- [72] D. Hong, Y. Tsukakoshi, H. Kotani, T. Ishizuka, K. Ohkubo, Y. Shiota, T. Kojima, *Inorg. Chem.* **2018**, *57*, 7180.

SUPPORTING INFORMATION

Additional supporting information may be found online in the Supporting Information section at the end of this article.

How to cite this article: Mohammadnezhad G, Abad S, Farrokhpour H, Görls H, Plass W. Electrocatalytic property, anticancer activity, and density functional theory calculation of [NiCl(P[^]N[^]P)]Cl.EtOH. *Appl Organomet Chem.* 2020; e6092. <https://doi.org/10.1002/aoc.6092>